



SPE 144355

Numerical Simulation of Shale-Gas Production: from Pore-Scale Modeling of Slip-Flow, Knudsen Diffusion, and Langmuir Desorption to Reservoir Modeling of Compressible Fluid

V. Shabro, C. Torres-Verdín, and F. Javadpour, The University of Texas at Austin

Copyright 2011, Society of Petroleum Engineers

This paper was prepared for presentation at the SPE North American Unconventional Gas Conference and Exhibition held in The Woodlands, Texas, USA, 14–16 June 2011.

This paper was selected for presentation by an SPE program committee following review of information contained in an abstract submitted by the author(s). Contents of the paper have not been reviewed by the Society of Petroleum Engineers and are subject to correction by the author(s). The material does not necessarily reflect any position of the Society of Petroleum Engineers, its officers, or members. Electronic reproduction, distribution, or storage of any part of this paper without the written consent of the Society of Petroleum Engineers is prohibited. Permission to reproduce in print is restricted to an abstract of not more than 300 words; illustrations may not be copied. The abstract must contain conspicuous acknowledgment of SPE copyright.

Abstract

We combine a new pore-scale model with a reservoir simulation algorithm to predict gas production in gas-bearing shales. It includes an iterative verification method of surface mass balance to ensure real-time desorption-adsorption equilibrium with gas production. The pore-scale model quantifies macroscopic petrophysical properties of formations using an algorithm of gas transport in porous media that simultaneously considers the effects of no-slip and slip flow, Knudsen diffusion, and Langmuir desorption. Subsequently, the reservoir model populates petrophysical properties derived from the pore-scale analysis at every numerical grid and at each time-step to calculate the production history and pressure distribution in the reservoir. This approach examines the contribution of different transport processes (i.e. advective flow, Knudsen diffusion, and desorption) to quantify their corresponding contributions to overall flow. Previously, we showed that slip flow and Knudsen diffusion play a significant role in explaining the higher-than-expected permeability observed in shale-gas formations with pore-throat sizes in the range of nanometers. It is shown that Langmuir desorption from organic-matter surfaces is important in the calculation of stored gas in gas-bearing shales. Modeling results show that gas desorption maintains the reservoir pressure via the supply of gas. In comparison to conventional reservoir descriptions, the contributions of slip flow and Knudsen diffusion increase the apparent permeability of the reservoir while gas production takes place. The effects of both mechanisms explain the higher-than-expected gas production rates commonly observed in these formations.

Introduction

Fossil fuels are perhaps the most significant sources of fossil fuel currently available. Despite increasing environmental consciousness that aims to diversify energy sources to mitigate global climate change, fossil fuels will continue to supply the majority of energy consumption throughout this century. Natural gas is the cleanest fossil fuel, but as a finite source, more challenging reservoirs must be explored to meet the growing world demand (Ground Water Protection Council and ALL Consulting 2009). In this situation, gas-bearing shale strata are important energy resources in North America and they will become increasingly important all over the world. Nevertheless, gas production in these formations has remained mostly unpredictable, which has caused their categorization as unconventional gas reserves (Passey et al. 2010).

Determining the petrophysical characteristics of a reservoir (e.g. permeability) and predicting production of gas-bearing shales is essential for economical assessments prior to field development. However, there is no standard model available to predict gas production from shale strata. Existing empirical and simplified models do not predict gas production accurately even though the production is usually higher than predictions made with conventional models (i.e. Darcy's equation) (Lu et al. 1995; Javadpour et al. 2007; Gault and Stotts 2007; Javadpour 2009; Sondergeld, et al. 2010; Ambrose et al. 2010; Kale et al. 2010; Sondergeld, et al. 2010; Freeman et al. 2010; Shabro et al. 2011). Recently, pore-scale characterization of shale formations using Focused Ion Beam-Scanning Electron Microscopy (FIB-SEM) and Atomic Force Microscopy (AFM) methods has advanced our understanding of shale morphologies and physical mechanisms behind gas production in these formations (Ambrose et al. 2010; Sondergeld et al. 2010; Javadpour 2009). At the same time, we have developed a pore-scale method to (1) analyze the imaged pore space; (2) characterize slip and no-slip flows, Knudsen diffusion and Langmuir desorption-adsorption; and (3) calculate apparent petrophysical properties (Shabro et al. 2009; Shabro et al. 2011). Apparent permeability depends on the smoothness of mineral grain surfaces, pressure, temperature, and gas molar mass as well as on pore-scale morphology. Gas and surface types, pressure, and temperature also control Langmuir desorption.

In this paper, our pore-scale model is combined with a modified reservoir-scale model to honor the suggested nano-scale physical transport mechanisms known to take place in shale-gas formations. The goal is to describe shale-gas production and model gas production in these formations from fundamental physical principles. In addition, we have developed a criterion to model gas desorption when a formation deviates from the equilibrium desorption-adsorption state during production. The presented model provides an evaluation of the significance of each transport mechanism in shale-gas production. It also offers a predictive tool for gas production performance within the constraint of existing physical understanding. Because it is based on fundamental fluid transport mechanisms, our simulation method provides an adequate physical understanding of gas production in shale formations. However, since the model is computationally ambitious, predictions are limited by the pore-scale characterization capabilities and the computational resources available; consequently, the presented predictions are at best qualitative in nature.

Firstly, compressible gas flow is modeled in a tube via the finite-difference method, taking into account the effects of slip and no-slip flows, Knudsen diffusion, and Langmuir desorption-adsorption. Subsequently, we invoke our pore-scale finite-difference method (Shabro et al. 2009; Shabro et al. 2011) to integrate the effects of slip and no-slip flows, Knudsen diffusion, and Langmuir desorption-adsorption. Next, the pore-scale model is combined with a one-dimensional radial reservoir model to appraise the effects of permeability variation and desorption when pressure is varied in the reservoir. The results and discussion section of this paper summarizes the combined effect of interplaying transport mechanisms. Finally, we evaluate and summarize the significance of the suggested mechanisms in the production of gas-bearing shales.

Gas Desorption and Flow in a Cylindrical Tube

We solve the equations of gas flow in a tube by taking into account the effects of no slip and slip-flow, Knudsen diffusion, and Langmuir desorption. The fundamental model in this section is extended in the next sections to develop complementary pore-scale and radial reservoir-scale descriptions that incorporate all the abovementioned flow mechanisms.

It was previously shown that slip-flow and Knudsen diffusion are important flow mechanisms in shale-gas formations. In doing so, we invoked different Knudsen regimes to differentiate shale-gas reserves from conventional gas reserves (Javadpour et al. 2007; Javadpour 2009; Shabro et al. 2009). Slip and no-slip flow mechanisms as well as Knudsen diffusion can be combined in one equation to model gas flow for both conventional and shale-gas formations (Javadpour 2009; Shabro et al. 2009). The gas flux equation in a cylindrical tube that takes into account Knudsen diffusion and advective gas flow is given by

$$J = - \left[\sqrt{\frac{8RT}{\pi M}} \left(\frac{2}{3RT\rho_{avg}} + \frac{\pi}{8\rho_{avg}} \left(\frac{2}{\alpha} - 1 \right) \right) r + \frac{r^2}{8\mu} \right] \frac{(P_2 - P_1)}{L}, \quad (1)$$

where J is volume flux, R is the universal gas constant, T is temperature, M is gas molar mass, P_1 and P_2 are pressures at the inlet and outlet of the tube, respectively, $p_{avg} [(P_1 + P_2)/2]$ is the average pressure, ρ_{avg} is average gas density, α is the tangential momentum accommodation coefficient, μ is gas viscosity, r is the tube radius, and L is the length of the tube. The first term between brackets in Eq. (1) represents diffusive flow and slip flow; the second term corresponds to conventional models. If the first term is neglected, Eq. 1 simplifies to Hagen-Poiseuille's equation and permeability is equal to $r^2/8$. On the other hand, when r decreases, the second term decreases more rapidly than the first term; this effect results in the increasing contribution of diffusion and slip flows to the total flow. Other characteristics of porous media and gas such as temperature, pressure, gas type and wall-surface smoothness influence the transition from conventional models (dominant second term) to increasing contribution of slip flow and Knudsen diffusion (dominant first term). Slip flow and diffusion become dominant flow mechanisms in formations with pore-throat sizes in the range of nano-meters (Javadpour 2009; Shabro et al. 2009).

We align a cylindrical tube in the x-direction and model diffusion, slip and no-slip flows along with Langmuir desorption in a one-dimensional (1-D) Cartesian framework. Mass conservation requires that the difference between influx and outflux be equal to the algebraic sum of generation and accumulation. The resulting mass balance is written as

$$\phi \frac{\partial \rho}{\partial t} + \nabla \cdot J = \rho F, \quad (2)$$

where ϕ is porosity ($\phi = 1$ for a tube), ρ is gas density, t is time, and F is the generation term. We assume that Langmuir desorption and adsorption are the sole contributions to the generation term in a shale-gas formation. In the presence of adsorbed gas on the tube wall, the generation term is the superposition of Langmuir desorption and adsorption mechanisms (Ruthven 1984). Desorption volume flux is defined by

$$J_{des} = K_{des} \theta, \quad (3)$$

where K_{des} is the desorption coefficient and θ is fractional coverage (the number of filled surface sites divided by the number of total surface sites available for gas molecules to adhere to the surface). Adsorption volume flux is expressed as

$$J_{ads} = K_{ads} (1 - \theta) P, \quad (4)$$

where K_{ads} is the adsorption coefficient, and $(1 - \theta)$ is the fractional vacancy (the number of unfilled surface sites divided by the number of total surface sites available for gas adsorption). The desorption flux is only dependent on material properties and the fractional coverage, while adsorption flux depends on material properties, fractional vacancy and also pressure. These two mechanisms (gas desorption and adsorption) are continually present and they nullify the effects of one another at equilibrium. Consequently, the fractional coverage at equilibrium is given by

$$\theta = \frac{K_{ads} P}{K_{des} + K_{ads} P}. \quad (5)$$

Equilibrium fractional coverage depends on pressure and surface-gas chemistry via K_{ads} and K_{des} . In a producing shale-gas reservoir, pressure drops cause desorption flux to surpass adsorption flux. The difference between these two fluxes gives rise to produced gas due to desorption. As a result, the generation term becomes

$$F = \frac{Surface}{Volume} (J_{des} - J_{ads}) = \frac{2\pi r x}{\pi r^2 x} (J_{des} - J_{ads}) = \frac{2}{r} (J_{des} - J_{ads}), \quad (6)$$

where x is the length of the tube. Figure 1 illustrates the interplay of the desorption-adsorption contributions with the input and output fluxes in a tube. By combining Eqs. 1 and 6 with Eq. 2, we describe the mass conservation, flow, and desorption mechanisms for a tube as

$$\phi \frac{\partial}{\partial t} \rho + \frac{\partial}{\partial x} \left(\rho \frac{k}{\mu} \cdot \frac{\partial}{\partial x} P \right) = \frac{2}{r} \rho (J_{des} - J_{ads}), \quad (7)$$

where k is apparent permeability, defined as (Javadpour 2009)

$$k = \left[\sqrt{\frac{8RT}{\pi M}} \left(\frac{2}{3RT\rho_{avg}} + \frac{\pi}{8p_{avg}} \left(\frac{2}{\alpha} - 1 \right) \right) r \mu + \frac{r^2}{8} \right]. \quad (8)$$

The equation of state transforms density to pressure in Eq. 7. By substituting Eqs. 3 and 4 in Eq. 7 we obtain

$$\phi \frac{\partial}{\partial t} \left(\frac{P}{z} \right) + \frac{\partial}{\partial x} \left(\frac{Pk}{z\mu} \cdot \frac{\partial}{\partial x} P \right) = \frac{2P}{zr} (K_{des}\theta - K_{ads}(1 - \theta)P), \quad (9)$$

where z is the gas compressibility factor. We assume that the gas compressibility factor is constant, whereby the gas compressibility factor is simplified from Eq. 9. This assumption is allowable in the modeled shale-gas reservoir in this paper. The simplified Eq. 9 is discretized to obtain

$$\phi \frac{P_{x,t+1} - P_{x,t}}{\Delta t} + \frac{k}{\mu \Delta x^2} (P_{x+1,t}^2 - 2P_{x,t}^2 + P_{x-1,t}^2) = \frac{2P_{x,t}}{r} (K_{des}\theta_{x,t} - K_{ads}(1 - \theta_{x,t})P_{x,t+1}), \quad (10)$$

where Δt and Δx are time-step and grid size, respectively. Gas viscosity is defined in each grid and can be updated with changes of pressure. If the fractional coverage ($\theta_{x,t}$) is identified, we find the solution explicitly from Eq. 10 to model gas flow and desorption mechanisms in a cylindrical tube.

The fractional coverage is iteratively solved at each step to satisfy the mass balance condition at the tube wall surface. Mass balance at the surface specifies that effective gas desorption flux must be consistently justified by the change in fractional coverage. Surface mass balance is formulated as

$$\rho (K_{des}\theta_{x,t} - K_{ads}(1 - \theta_{x,t})P_{x,t+1}) \Delta t = \frac{S_0 M}{N_A} (\theta_{x,t} - \theta_{x,t+1}), \quad (11)$$

where S_0 is the number of total surface sites available for gas adsorption per surface area, M is the gas molar mass, and N_A is the Avogadro constant. The left hand side of Eq. 11 is the mass of the generated gas calculated from the modeled gas desorption and adsorption terms, whereas the right-hand side of Eq. 11 stands for the mass of generated gas due to changes in fractional coverage when pressure decreases.

The following algorithm is used to identify fractional coverage iteratively. Assuming that the reservoir is at equilibrium at initial conditions, the initial fractional coverage in the first time-step is calculated from Eq. 5 at the initial pressure. The new pressure ($P_{x,t+1}$) is found explicitly from Eq. 10, and the new fractional coverage ($\theta_{x,t+1}$) is calculated via Eq. 5 at the new pressure. If the surface mass balance (Eq. 11) is satisfied within an error margin (equal to 1% in our simulations), the model is advanced to the next time-step. On the other hand, if surface mass balance is not satisfied, then the desorption and adsorption coefficients (K_{des} and K_{ads}), or the fractional coverage ($\theta_{x,t+1}$) are modified to honor surface mass balance.

If the left-hand side of Eq. 11 exceeds the right hand side, the modeled desorption process has surpassed the possible gas generation due to pressure drop. To counteract this problem, the new desorption and adsorption coefficients (K_{des_new} and K_{ads_new}) for that specific calculation of $P_{x,t+1}$ are revised using the relationship

$$\frac{K_{des_new}}{K_{des_old}} = \frac{K_{ads_new}}{K_{ads_old}} = \left[\frac{S_0 M}{N_A} (\theta_{x,t} - \theta_{x,t+1}) \right] / \left[\rho (K_{des} \theta_{x,t} - K_{ads} (1 - \theta_{x,t}) P_{x,t+1}) \Delta t \right], \quad (12)$$

and $P_{x,t+1}$ and $\theta_{x,t+1}$ are calculated again using Eq. 10. This condition occurs in formations with low permeability and high desorption rates.

Conversely, if the right-hand side of Eq. 11 exceeds the left-hand side, possible gas generation due to pressure drop has surpassed the modeled desorption process. To offset this effect, the fractional coverage ($\theta_{x,t+1}$) is updated via

$$\theta_{x,t+1} = \theta_{x,t} - \rho (K_{des} \theta_{x,t} - K_{ads} (1 - \theta_{x,t}) P_{x,t+1}) \frac{\Delta t N_A}{S_0 M}, \quad (13)$$

thereby securing convergence. This latter condition takes place in formations with high permeability and low desorption rates. It also arises at the near-wellbore region where pressure varies significantly in short periods of time.

Figure 2 shows a flowchart of the implementation of the iterative method and surface mass balance using Eqs. 11, 12 and 13 combined with Eq. 10. We readily assess the contribution of desorption by disregarding the generation term, F , in Eq. 6 for cases without desorption.

Pore-Scale Modeling of Gas Desorption and Flow

We previously introduced a pore-scale model based on finite-difference modeling of pressure distributions at the pore-scale to model flow and estimate permeability in porous media and studied the effects of no-slip and slip flow, Knudsen diffusion and Langmuir desorption-adsorption at the pore-scale (Shabro et al. 2009; Shabro et al. 2011). Flow contributions due to slip flow and Knudsen diffusion rapidly increase when the pore-throat sizes decrease to the nano-meter range and apparent permeability is defined to account for these contributions (Javadpour 2009; Shabro et al. 2009). Equation 8 describes important parameters in calculating the apparent permeability in a tube excluding complexities due to realistic morphologies of porous media. Moreover, we showed that gas generation due to Langmuir desorption-adsorption does not change permeability significantly; however we predicted that it could have a direct effect on pressure maintenance in porous media (Shabro et al. 2011). These models are applied here to calculate fundamental properties of porous media. In particular, a cemented grain-pack represents the pore-scale image of a shale-gas formation. Then, porosity and surface-to-volume ratio (χ) are calculated via image analysis, and permeability is modeled with our finite-difference pore-scale model at each time-step and in each grid. We interpolate the petrophysical properties of porous media when pressure changes are small in order to decrease the total simulation time. A typical permeability variation with pressure is shown in Fig. 3 for a grain-pack with a smallest throat diameter equal to 10 nm, porosity of 8.45% and surface-to-volume ratio equal to $3.29 \times 10^9 \text{ m}^{-1}$. This grain-pack will be used as a model of a shale-gas pore-scale image.

Combined Pore-Scale and Reservoir Modeling of Radial Gas Flow

We develop a 1-D radial gas flow model based on the simulation schemes for the 1-D tube model to incorporate the effect of Langmuir desorption-adsorption terms. Equation 9 is written as

$$\phi \frac{\partial}{\partial t} P + \frac{1}{r} \frac{\partial}{\partial r} \left(r \frac{k}{\mu} P \frac{\partial}{\partial r} P \right) = \chi P (K_{des} \theta - K_{ads} (1 - \theta) P), \quad (14)$$

where porosity, permeability and surface-to-volume ratio and desorption and adsorption coefficients are calculated from the pore-scale model described in the previous section. Figure 4 is a schematic of the combined pore-scale and reservoir models of 1-D radial gas flow. Surface mass balance is achieved iteratively via Eqs. 11, 12 and 13. Figure 2 shows a flowchart of the two combined models including surface mass balance.

The value of Δt is updated at each time-step to ensure convergence of results. This step is achieved by increasing Δt to twice the value when all the changes in pressure are below 0.0001% in the relevant time-step and by decreasing Δt to half the value when at least one of the changes in pressure is above 0.01% in the relevant time-step. Convergence of the resulting model is tested by refining the grids in the radial direction (and consequently, by refining the time-steps) and comparing the result of production after a certain time. Figure 5 shows that simulated cumulative gas productions converge after a few grid refinement steps of approximately 100 grids in the radial direction for this case. Other modeling results such as pressure and production converge after a few grid refinement steps.

Results and Discussion

First, we investigated the effect of desorption, slip flow and Knudsen diffusion in a cylindrical tube as a simplified model of gas transport in porous media. Figure 6 shows the cumulative production from a tube with radius equal to 2 nm. Corresponding modeling parameters are listed in Table 1. If desorption is taken into account, production will increase by 38% after 10 years. The resulting permeability for this tube is 1479 nd from Eq. 8. If a bundle of tubes is constructed with the 2 nm tube and porosity is 8.45%, permeability would be equal to 125 nd. If slip flow and Knudsen diffusion are neglected, the conventional permeability will become three times smaller, equal to 507 nd and 43 nd, respectively.

In the next step, we used a grain-pack of 8.45% porosity to model shale-gas formations using the physical parameters listed in Table 1. With the smallest throat size equal to 5 nm, the resulting permeability from the pore-scale model varies between 250 nd and 347 nd, while the conventional permeability is invariably 188 nd. Figure 7a compares production curves obtained with the combined pore-scale and reservoir models for the cases when permeability is assumed constant or dependent on pressure, as well as for the cases with and without desorption. The effect of desorption almost doubles the cumulative production whereas the production rate decreases more slowly than the case without desorption. Likewise, both production rate and cumulative production increase when we take into account the pressure dependency of permeability, but less significantly (about 15%). Nonetheless, if the conventional permeability is used, cumulative production will decrease by approximately 33%. In Fig. 7b, we observe the production rate for a longer period of time for the cases with and without desorption. Figure 8 shows pressure distributions in the reservoir after 1 and 50 years of production with and without desorption. Gas desorption maintains the reservoir pressure, and consequently, it increases production rate and cumulative production in shale-gas reservoirs.

Our modeling results suggest that desorption is the principal mechanism for higher-than-expected production rates and longer production lives commonly observed in shale-gas reservoirs compared to conventional reservoirs. Desorption effects increase with organic matter content because organic matter is gas-absorbent and it causes the number of total surface sites to increase. The high surface-to-volume ratio amplifies desorption as well. In addition, slip flow and Knudsen diffusion increase permeability in the nano-scale pores and throats of porous media, thereby giving rise to higher production rate of free gas than predicted by conventional reservoir simulation models. Apparent permeability increases with pressure drop when slip flow and Knudsen diffusion are the prevailing flow mechanisms. It is therefore important that the two mechanisms be taken into consideration in reservoir evaluations of gas-bearing shales.

Conclusions

We combined a previously developed pore-scale model with a modified reservoir simulation algorithm to predict production in gas-bearing shales. The description simultaneously takes into account the effects of no-slip and slip flow, Knudsen diffusion, and desorption. In doing so, we introduced a new surface mass balance mechanism to model transient desorption. It was found that apparent permeability was higher than conventional permeability in shale-gas formations due to slip flow and Knudsen diffusion. Results also indicated that apparent permeability increased during production. Desorption of gas maintains reservoir pressure for a longer period of time, thereby increasing both gas production rates and the life of the reservoir. The effects of these two fluid transport mechanisms are consistent with higher-than-expected gas production rates and longer gas production periods commonly observed in gas-bearing shales.

Acknowledgements

The authors thank Kamy Sepehrnoori and Rooholah Abdollah Pour from the University of Texas at Austin (UT Austin) for their instructive comments and discussions, and Mohammad Moravvej with the NanoGeosciences Laboratory at UT Austin's Bureau of Economic Geology for the AFM image. The work reported in this paper was funded by UT Austin's Research Consortium on Formation Evaluation, jointly sponsored by Anadarko, Apache, Aramco, Baker-Hughes, BG, BHP Billiton, BP, Chevron, ConocoPhillips, ENI, ExxonMobil, Halliburton, Hess, Maersk, Marathon, Mexican Institute for Petroleum, Nexen, Pathfinder, Petrobras, Repsol, RWE, Schlumberger, Statoil, TOTAL, and Weatherford.

Nomenclature

1-D	One-dimensional
AFM	Atomic Force Microscopy
F	Generation term, s^{-1}
FIB-SEB	Focused Ion Beam-Scanning Electron Microscopy
J	Volume flux, $m.s^{-1}$
J_{ads}, J_{des}	Adsorption and desorption volume flux, $m.s^{-1}$
k	Permeability, m^2 [$d = \text{Darcy} = 9.869 \times 10^{-13} m^2$]
K_{ads}	Adsorption coefficient, $m.Pa^{-1}.s^{-1}$
K_{des}	Desorption coefficient, $m.s^{-1}$
L	Porous media (tube) length, m
M	Molar mass, $kg.kmol^{-1}$
N_A	Avogadro constant, $6.0221415 \times 10^{23} mol^{-1}$
P, P_1, P_2	Pressure, Pa
P_{avg}	Average pressure, Pa
R	Universal gas constant, $8.314 \times 10^3 Pa.m^3.kmol^{-1}.K^{-1}$
r	Tube radius, or radial length parameter, m
S_0	Number of total surface sites available for gas adsorption per surface area, m^{-2}
T	Temperature, K
t	time, s
x	Tube length, or Cartesian length parameter, m
z	Gas compressibility factor, dimensionless
α	Tangential momentum accommodation coefficient, dimensionless
θ	Fractional coverage, dimensionless
μ	Viscosity, $Pa.s$
ρ	Gas density, $kg.m^{-3}$
ρ_{avg}	Average fluid gas, $kg.m^{-3}$
ϕ	Porosity, dimensionless
χ	Surface-to-volume ratio, m^{-1}

References

- Ambrose, R. J., Hartman, R. C., Diaz-Campos, M., Akkutlu, I. Y., and Sondergeld, C. H. 2010. New Pore-scale Considerations for Shale Gas in Place Calculations. SPE-131772, paper presented at the Unconventional Gas Conference, SPE, Pittsburgh, PA, 23-25 February.
- Freeman, C. M., Moridis, G., Ilk, D., and Blasingame, T. 2010. A Numerical Study of Transport and Storage Effects for Tight Gas and Shale Gas Reservoir Systems. SPE-131583, paper presented at the International Oil and Gas Conference and Exhibition, SPE, Beijing, China, 8-10 June.
- Gault, B., and Stotts, G. 2007. Improve Shale Gas Production Forecasts. *Hart's Exploration & Production*, v. 80, pp. 85-87.
- Ground Water Protection Council, and ALL Consulting. 2009. Modern Shale Gas Development in the United States: A Primer. *Prepared for the Department of Energy Office of Fossil Energy and National Energy Technology Laboratory, Washington DC*.
- Javadpour, F. 2009. Nanopores and Apparent Permeability of Gas Flow in Mudrocks (Shales and Siltstone). *J. of Canadian Petroleum Tech.*, v. 48, pp. 16-21.
- Javadpour, F., Fisher, D., and Unsworth, M. 2007. Nanoscale Gas Flow in Shale Gas Sediments. *J. of Canadian Petroleum Tech.*, v. 46, pp. 55-61.
- Kale, S. V., Rai, C. S., and Sondergeld, C. H. 2010. Petrophysical Characterization of Barnett Shale. SPE-131770, paper presented at the Unconventional Gas Conference, SPE, Pittsburgh, PA, 23-25 February.
- Lu, X. C., Li, F. C., and Watson, A. T. 1995. Adsorption Measurements in Devonian Shales. *Fuel*, v. 74, pp. 599-603.

- Passey, Q. R., Bohacs, K. M., Esch, W. L., Klimentidis, R., and Sinha, S. 2010. From Oil-Prone Source Rock to Gas-Producing Shale Reservoir-Geologic and Petrophysical Characterization of Unconventional Shale Gas Reservoirs. SPE-131350, paper presented at the International Oil and Gas Conference and Exhibition, SPE, Beijing, China, 8-10 June.
- Ruthven, D. M. 1984. *Principles of adsorption and adsorption processes*. Wiley-Interscience.
- Shabro, V., Javadpour, F., and Torres-Verdín, C. 2009. A Generalized Finite-Difference Diffusive-Advective (FDDA) Model for Gas Flow in Micro- and Nano-Porous Media. *World Journal of Engineering*, v. 6 (3), 7-15.
- Shabro, V., Torres-Verdín, C., and Javadpour, F. 2011. Pore-Scale Modeling of Slip Flow, Knudsen Diffusion, and Langmuir Desorption to Estimate Apparent Permeability in Shale-Gas Formations. *Society of Petrophysicists and Well-Log Analysts*, Colorado Springs, CO, 15-18 May.
- Sondergeld, C. H., Ambrose, R. J., Rai, C. S., and Moncrieff, J. 2010. Micro-Structural Studies of Gas Shales. SPE-131771, paper presented at the Unconventional Gas Conference, SPE, Pittsburgh, PA, 23-25 February.
- Sondergeld, C. H., Newsham, K. E., Comisky, J. T., Rice, M. C., and Rai, C. S. 2010. Petrophysical Considerations in Evaluating and Producing Shale Gas Resources. SPE-131768, paper presented at the Unconventional Gas Conference, SPE, Pittsburgh, PA, 23-25 February.

Table 1. Summary of modeling parameters assumed in the calculations reported in this paper.

r (nm)	2
μ (Pa.s) $\times 10^5$	1.75
ρ_{initial} (kg.m ⁻³)	78.9
K_{ads} (m.Pa ⁻¹ .s ⁻¹)	3.7×10^{19}
K_{des} (m.s ⁻¹)	7×10^{13}
α	0.8
M (kg.kmol ⁻¹)	16
T (K)	423
L (m)	100
P_{initial} (MPa)	17.2
P_{final} (MPa)	8.6
ϕ	8.45%
χ (m ⁻¹)	3.29×10^9
S_0 (m ⁻²)	7.3×10^{18}

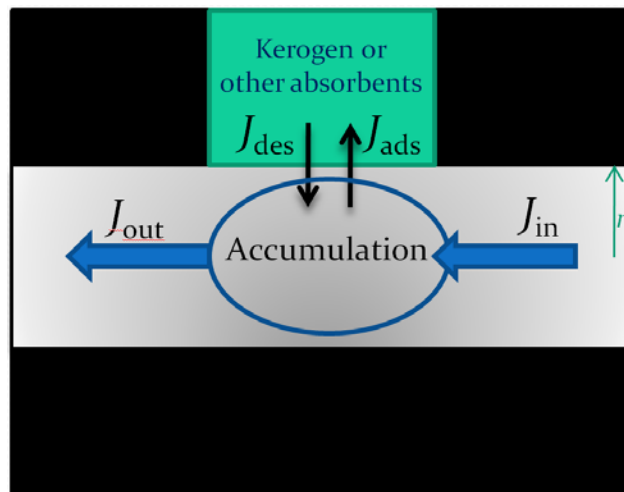


Fig. 1. Desorption-adsorption contributions to flow in a tube. Output flux is the superposition of input flux, effective desorption (desorption flux minus adsorption flux) and the change in accumulated gas in the tube due to pressure variations.

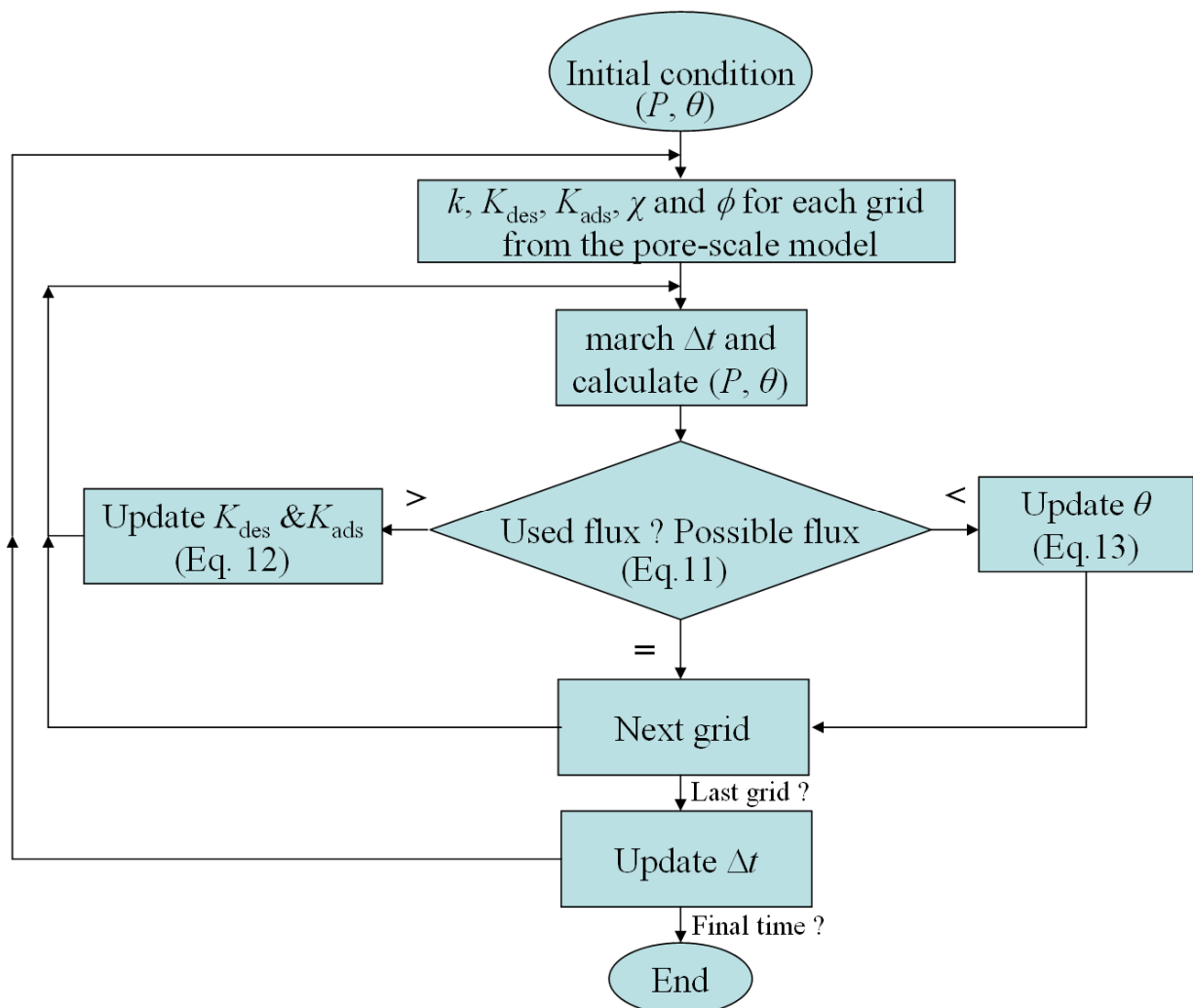


Fig. 2. Flowchart describing the iterative implementation of surface mass balance and the combined reservoir and pore-scale modeling of production in shale-gas formations.

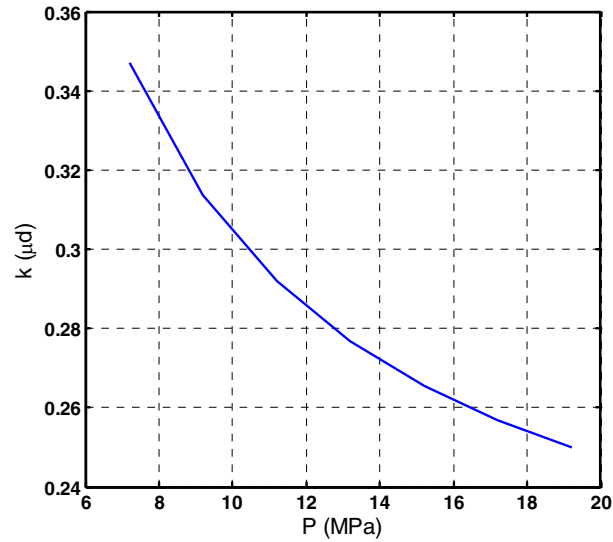


Fig. 3. Permeability variation versus pressure from pore-scale modeling of a grain-pack with 8.45% porosity with smallest throat sizes (diameter) equal to 10 nm. Permeability varies from 250 nd to 347 nd when pressure decreases from 19.2 MPa to 7.2 MPa.

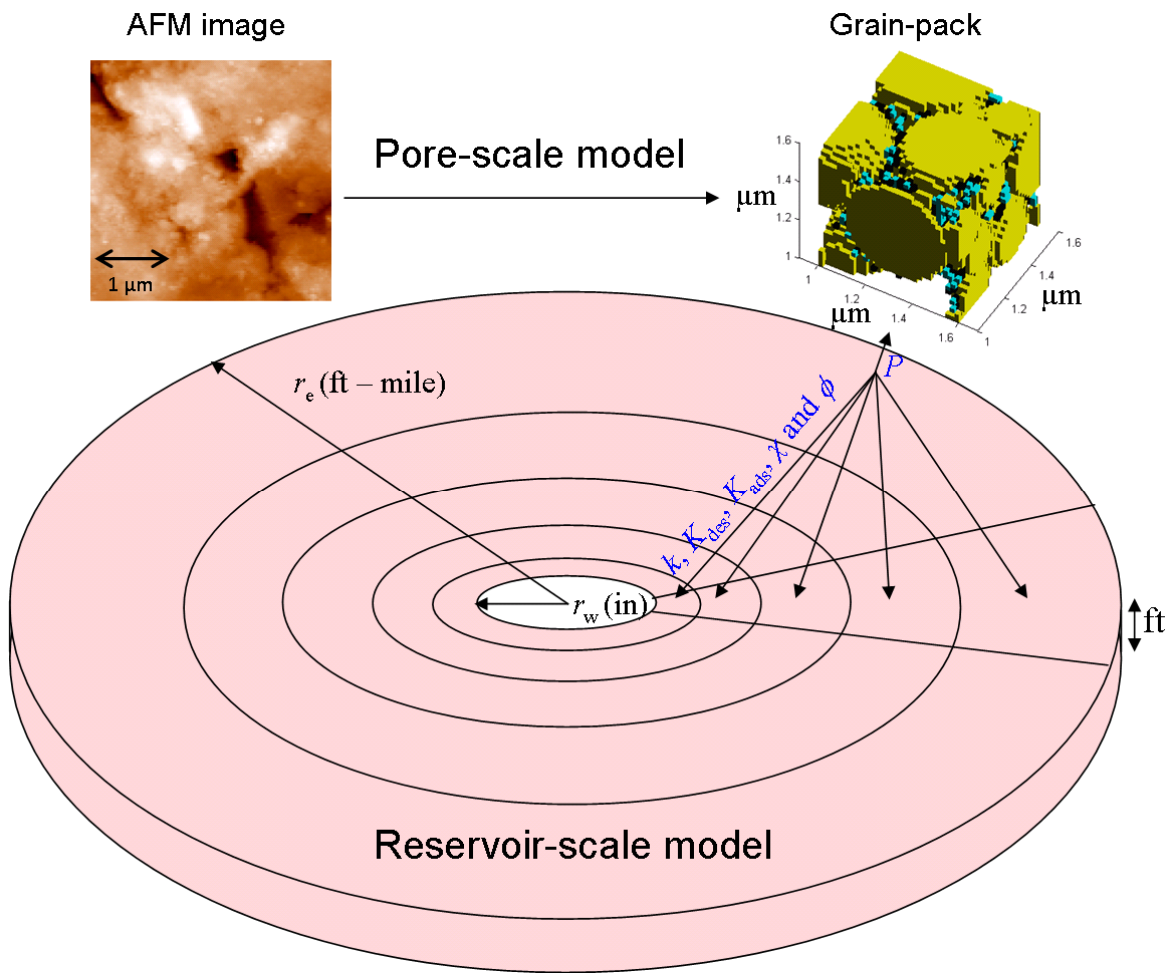


Fig. 4. Schematic of the combined pore- and reservoir-scale models of 1-D radial gas flow. The pore-scale model provides the required petrophysical parameters for each grid of the reservoir model, whereas and the reservoir model updates the pressure at each time-step. Representative images of shale-gas formations from grain-packs, AFM, or FIB-SEM are input to the pore-scale model.

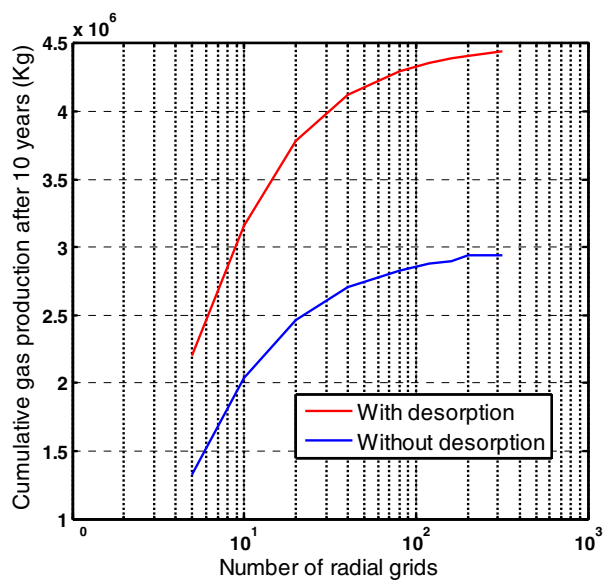


Fig. 5. Convergence diagnostic of the pore-scale/reservoir-scale simulation model. Production converges after a few grid refinement steps.

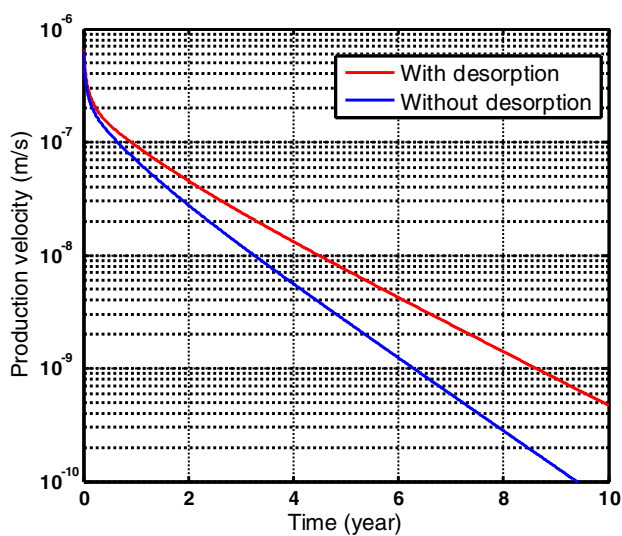


Fig. 6. Production curves for a tube with radius equal to 2 nm ($\chi = 10^9 \text{ m}^{-1}$). After 10 years, cumulative production for the case of desorption is 38% higher than cumulative production for a tube without desorption. Table 1 summarizes the remaining assumed modeling parameters.

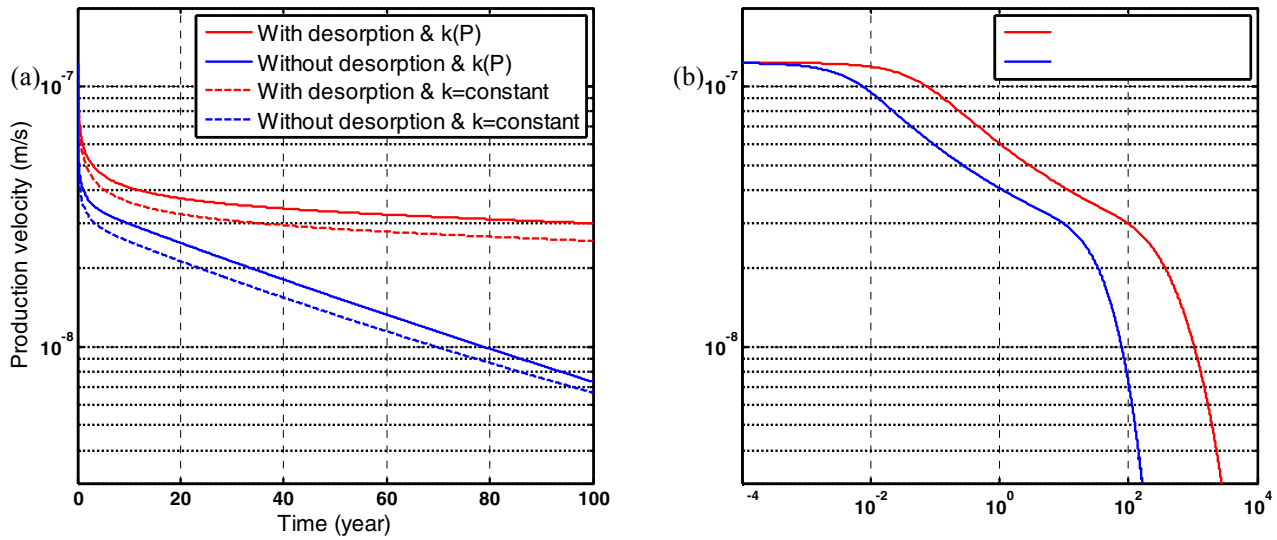


Fig. 7. Production curves of a shale-gas reservoir constructed from representative grain-packs with 8.45% porosity. (a) Cumulative production increases 15% and 95% compared to conventional model (dashed blue line) in the cases of added pressure dependency of permeability (solid blue line) and desorption (dashed red line), respectively. When both effects are present (red line), cumulative production increases 122% compared to conventional models. Production decreases more gradually in the case with desorption than without desorption. (b) Production rates for a longer period of time are shown for the cases with and without desorption. Production comes to an end faster in the case without desorption than in the case when desorption is taken into account. This behavior indicates that desorption is responsible for the longer life of shale-gas reservoirs compared to conventional reservoirs. Table 1 describes the assumed modeling parameters.

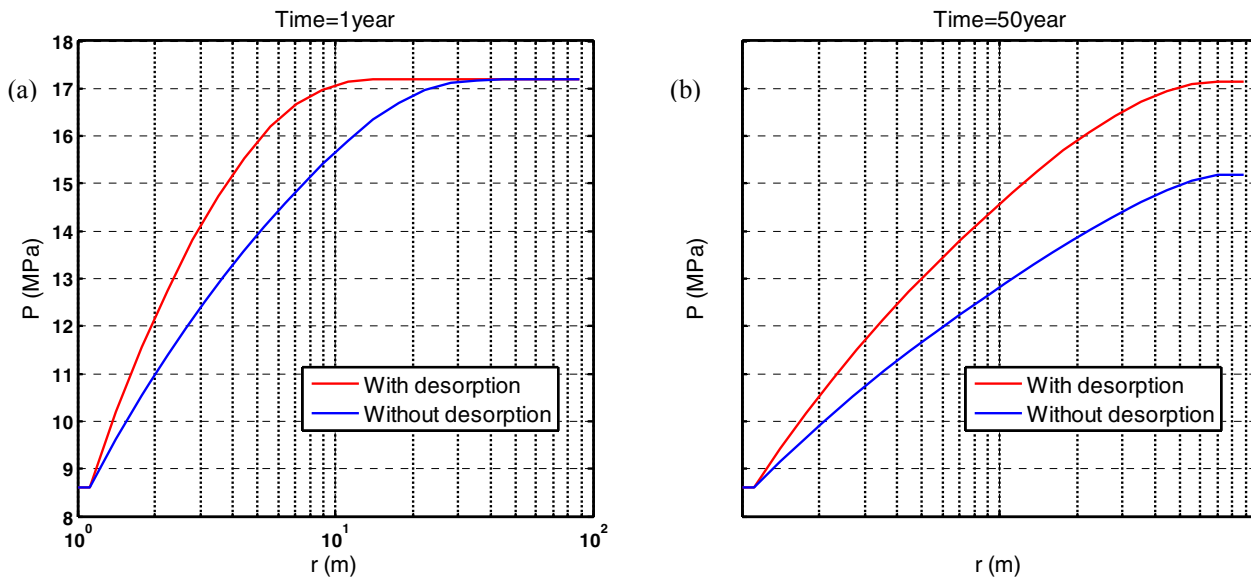


Fig. 8. Radial profiles of pressure after (a) 1 year and (b) 50 years of production from results shown in Fig. 7. Desorption maintains reservoir pressure, whereby it increases production rate and cumulative production in shale-gas reservoirs.